Research Square

Preprints are preliminary reports that have not undergone peer review.
They should not be considered conclusive, used to inform clinical practice,
or referenced by the media as validated information.

Coelastrella sp. extract attenuates inflammatory responses and NF-κB p65 nuclear accumulation in LPS- stimulated RAW 264.7 macrophages

Su Jeong Hwang
hsj9876543@gmail.com
Sun Moon University
Ju Hwan Lee
Sun Moon University
Jong Hyun Oh
Sun Moon University
Do Hyeon Jin
Sun Moon University
Seung Won Nam
Nakdonggang National Institute of Biological Resources
Jin Woo Kim
Sun Moon University
Sunhye Lee
Sun Moon University

Article

Keywords: Coelastrella sp., anti-inflammatory activity, RAW 264.7 macrophages, NF-κB p65, oxidative stress

Posted Date: September 21st, 2026

DOI: https://doi.org/10.21203/rs.3.rs-10703929/v1

License: This work is licensed under a Creative Commons Attribution 4.0 International License.
Read Full License

Additional Declarations: No competing interests reported.

Coelastrella sp. extract attenuates inflammatory responses and NF-κB p65 nuclear accumulation in LPS-stimulated RAW 264.7 macrophages

Su Jeong Hwang[1], Ju Hwan Lee[1], Jong Hyun Oh[1], Do Hyeon Jin[1],

Seung Won Nam[2], Jin Woo Kim[1,3*], Sunhye Lee[1*]

[1]Division of Food Technology and Nutrition, Sun Moon University, 70 Sunmoon-ro 221beon-gil, Tangjeong-myeon, Asan-si, Chungcheongnam-do 31460, Republic of Korea

[2]Freshwater Bioresources Culture Collection, Nakdonggang National Institute of Biological Resources, Sangju 37242, Republic of Korea

[3]Bombicola Inc., RM 1006, 10F, Bldg E, 30 Songdomirae-ro, Yeonsu-gu, Incheon 21990, Republic of Korea

**Jin Woo Kim and Sunhye Lee contributed equally to this study as corresponding authors*.

*Corresponding author:

Sunhye Lee

E-mail: Lsh71300@sunmoon.ac.kr

Abstract

This study investigated the anti-inflammatory effects of an extract obtained from *Coelastrella* sp. using 50% ethanol (CSE) in lipopolysaccharide (LPS)-stimulated RAW 264.7 macrophages. CSE contained 9.0 mg gallic acid equivalents/g dry matter of total polyphenols and 8.3 mg quercetin equivalents/g dry matter of total flavonoids and exhibited 2,2-diphenyl-1-picrylhydrazyl (DPPH) and 2,2′-azino-bis(3-ethylbenzothiazoline-6-sulfonic acid) (ABTS) radical-scavenging activities of 30.0% and 55.0%, respectively. CSE showed no significant cytotoxicity at 0.02–0.06 mg dry biomass equivalents/mL. In LPS-stimulated cells, CSE reduced nitrite accumulation, an indicator of nitric oxide production, by 10.6–32.7% and reactive oxygen species-associated fluorescence by 4.8–25.4%. CSE decreased mRNA expression of inducible nitric oxide synthase (*iNOS*), interleukin-6 (*IL-6*), interleukin-1β (*IL-1β*), tumor necrosis factor-α (*TNF-α*), and nuclear factor kappa B (*NF-κB*) by up to 46.1%, 13.1%, 65.1%, 33.9%, and 30.4%, respectively. At 0.06 mg dry biomass equivalents/mL, iNOS, IL-6, IL-1β, TNF-α, and NF-κB p65 protein levels decreased by 42.1%, 21.2%, 66.1%, 18.8%, and 62.8%, respectively. CSE also reduced nuclear NF-κB p65 fluorescence intensity by 10.1–57.1%. These findings indicate that CSE attenuates LPS-induced inflammatory responses, accompanied by reductions in oxidative stress-associated responses, nitrite accumulation, inflammatory marker expression, and NF-κB p65 nuclear accumulation.

Keywords: *Coelastrella* sp.; anti-inflammatory activity; RAW 264.7 macrophages; NF-κB p65; oxidative stress

1. Introduction

Inflammation is a fundamental physiological process that plays a critical role in initiating innate and adaptive immune responses while maintaining tissue homeostasis. It enables the elimination of harmful stimuli and supports tissue repair through a tightly regulated biological response to external pathogens or tissue injury. However, excessive activation of inflammatory pathways or inadequate resolution of inflammation can result in immune dysregulation and persistent tissue damage, thereby constituting a pathological basis for a wide range of chronic diseases. Chronic inflammation is widely recognized as a common underlying mechanism contributing to the initiation and progression of metabolic disorders, cardiovascular diseases, neurodegenerative conditions, and autoimmune diseases. In particular, sustained inflammatory states disrupt redox homeostasis within the tissue microenvironment, leading to the excessive accumulation of reactive oxygen species (ROS) [1]. Elevated ROS levels further potentiate pro-inflammatory signaling cascades, including nuclear factor kappa B (NF-κB), thereby establishing a self-amplifying cycle that accelerates pathological progression [2]. Consequently, increasing attention has focused on strategies that precisely regulate the magnitude and temporal dynamics of inflammatory signaling to restore equilibrium within the immune–metabolic–oxidative stress axis [3]. Such strategies represent an emerging therapeutic approach for reestablishing inflammatory homeostasis and ultimately preventing or attenuating the progression of chronic inflammatory diseases.

Macrophages are central effector cells of the innate immune system, orchestrating the initiation, amplification, and resolution of inflammatory responses while maintaining immune homeostasis. Upon activation by external stimuli such as lipopolysaccharide (LPS), a bacterial pathogen-associated molecular pattern, macrophages produce pro-inflammatory cytokines, including tumor necrosis factor-α (TNF-α), interleukin-6 (IL-6), and interleukin-1β (IL-1β), and induce the expression of inflammatory mediators such as inducible nitric oxide synthase (iNOS), cyclooxygenase-2 (COX-2), and microsomal prostaglandin E_2 synthase-1 (mPGES-1) [4]. The transcription of these inflammatory genes is tightly regulated by the NF-κB signaling pathway, a central regulator of macrophage inflammatory responses [5]. Under resting conditions, NF-κB is sequestered in the cytoplasm by inhibitor of κBα (IκBα). Upon LPS-induced activation of Toll-like receptor 4 (TLR4), IκBα is phosphorylated by the IκB kinase (IKK) complex and subsequently degraded via the ubiquitin–proteasome system, allowing NF-κB to translocate into the nucleus and activate the transcription of pro-inflammatory genes [6]. Based on this well-characterized mechanism, LPS-stimulated RAW 264.7 murine macrophages are widely used as an *in vitro* model for investigating NF-κB-mediated inflammatory signaling

and transcriptional regulation [7].

Commonly used anti-inflammatory agents in clinical practice, including non-steroidal anti-inflammatory drugs (NSAIDs) such as ibuprofen, naproxen, and indomethacin, as well as corticosteroids such as prednisolone and dexamethasone, effectively alleviate inflammatory symptoms. However, long-term administration is associated with adverse effects, including gastrointestinal mucosal injury, systemic immunosuppression, metabolic disturbances such as hyperglycemia and osteoporosis, and tissue atrophy [8]. These limitations are particularly important in patients with chronic inflammatory conditions, thereby restricting the long-term clinical use of conventional anti-inflammatory therapies. Meanwhile, biologic agents targeting key inflammatory mediators, such as TNF-α, IL-6, and IL-1β, including infliximab, adalimumab, and tocilizumab, have demonstrated efficacy in autoimmune and inflammatory diseases. Nevertheless, these biologics present several limitations, including high treatment costs, increased infection risk, restricted applicability to specific patient populations, and limited capacity to regulate complex inflammatory networks [9].

In this context, naturally derived bioactive resources have attracted increasing attention as complementary candidates for modulating inflammatory responses with relatively broad biochemical diversity. Among these resources, microalgae are photosynthetic microorganisms capable of producing diverse bioactive metabolites, including phenolic compounds, flavonoids, pigments, fatty acids, and other antioxidant-related constituents. These compounds have been associated with antioxidant and inflammation-modulatory activities, suggesting that microalgae may provide valuable sources for the development of functional ingredients targeting oxidative stress-associated inflammatory responses [10]. *Coelastrella* sp. is a freshwater green microalga with potential as a bioresource for functional compound development. However, despite growing interest in microalgae-derived bioactive materials, the anti-inflammatory effects of *Coelastrella* sp. extract (CSE) and its regulatory effects on ROS generation, NO production, and NF-κB-associated signaling in macrophages remain insufficiently characterized. Therefore, this study aimed to evaluate the anti-inflammatory activity of CSE in LPS-stimulated RAW 264.7 macrophages and to investigate whether its effects are associated with changes in intracellular ROS-associated fluorescence, nitrite accumulation, inflammation-related gene and protein expression, and NF-κB p65 nuclear accumulation.

2. Materials and methods

2.1. Microalgal pretreatment and ultrasound-assisted extraction

Freeze-dried *Coelastrella* sp. FBCC-A514 powder was obtained from the Freshwater Bioresources Culture Collection, Nakdonggang National Institute of Biological Resources (Sangju, Korea). One gram of the sample was extracted with 20 mL of 50% (v/v) ethanol (Samchun, Pyeongtaek, Korea) using an ultrasonic extractor (SD-D250H, Mujigae Co., Ltd., Seoul, Korea) operated at 40 kHz and 60 °C for 30 min, followed by centrifugation at 2,800 × g for 10 min (Labogene 1236R, Gyrozen, Daejeon, Korea). The resulting supernatant was collected, stored at 4 °C until further analysis, and used for subsequent experiments [11,12]. The concentration of CSE used in subsequent experiments was expressed as the dry weight equivalent of the freeze-dried microalgal powder used for extraction, not as the dry weight of the dried extract. Therefore, the extract prepared from 1 g of freeze-dried powder in 20 mL of solvent corresponded to 50 mg dry biomass equivalents/mL.

2.2. Analysis of secondary metabolite content

Total polyphenol content (TPC) and total flavonoid content (TFC) were determined using the Folin–Ciocalteu method and the aluminum chloride colorimetric assay [13,14]. Absorbance was measured at 765 nm and 415 nm using a UV–Vis spectrophotometer (Optizen 2120 UV, Mecasys, Korea). Quantification was performed using calibration curves generated with gallic acid and quercetin, and the results were expressed as mg gallic acid equivalents (GAE)/g dry matter (DM) and mg quercetin equivalents (QE)/g DM, respectively. Tannic acid (TA) was used as a reference compound.

2.3. Analysis of antioxidant activity (DPPH and ABTS assays)

Antioxidant activity was evaluated using the 2,2-diphenyl-1-picrylhydrazyl (DPPH) and 2,2′-azino-bis(3-ethylbenzothiazoline-6-sulfonic acid) (ABTS) radical-scavenging assays [15–17]. CSE was reacted with each radical solution under dark conditions, and absorbance was measured at 517 nm for DPPH and 734 nm for ABTS using a UV–Vis spectrophotometer (Optizen 2120 UV, Mecasys, Korea). Radical-scavenging activity was expressed as a percentage relative to the control, and ascorbic acid (AA) was used as a positive control.

$$\text{DPPH radical} - \text{scavenging activity (\%)} = \left(1 - \frac{\text{Absorbance of sample}}{\text{Absorbance of control}}\right) \times 100 \quad (1)$$

$$\text{ABTS radical} - \text{scavenging activity (\%)} = \left(1 - \frac{\text{Absorbance of sample}}{\text{Absorbance of control}}\right) \times 100 \quad (2)$$

2.4. Cell culture and cell viability assay

RAW 264.7 murine macrophages (Korean Cell Line Bank, Seoul, Korea) were cultured in Dulbecco's Modified Eagle's Medium (DMEM; Gibco, Waltham, MA, USA) supplemented with 10% fetal bovine serum and 1% penicillin–streptomycin at 37 °C in a humidified atmosphere containing 5% CO_2. Cell viability was evaluated using the 3-(4,5-dimethylthiazol-2-yl)-2,5-diphenyltetrazolium bromide (MTT) assay [18]. Cells were treated with CSE at concentrations ranging from 0 to 0.5 mg dry biomass equivalents/mL for 24 h. Subsequently, MTT solution (0.25 mg/mL) was added, and the cells were incubated for an additional 4 h. The resulting formazan crystals were dissolved in dimethyl sulfoxide (DMSO), and absorbance was measured at 570 nm. Cell viability was expressed relative to the untreated control.

$$\text{Cell viability (\%)} = \left(\frac{\text{Absorbance of the CSE} - \text{treated group}}{\text{Absorbance of the untreated control group}}\right) \times 100 \quad (3)$$

2.5. Analysis of nitrite accumulation

Nitrite (NO_2^-) accumulation, used as an indicator of nitric oxide (NO) production, was measured in culture supernatants using the Griess assay [19]. The Griess reagent was prepared by mixing equal volumes of 1% (w/v) sulfanilamide and 0.1% (w/v) N-(1-naphthyl)ethylenediamine dihydrochloride. RAW 264.7 macrophages were stimulated with LPS (1 μg/mL) and treated with CSE (0.02–0.06 mg dry biomass equivalents/mL) for 24 h; the LPS-treated control received no CSE. Culture supernatants were then collected and incubated with the Griess reagent at room temperature for 10 min. Absorbance was measured at 540 nm, and nitrite concentrations were calculated from a sodium nitrite standard curve. For graphical presentation, nitrite levels were normalized to the LPS-treated control and expressed as a percentage of the LPS-treated control.

2.6. Intracellular ROS measurement by flow cytometry

Intracellular ROS generation was evaluated using CellROX™ Orange staining followed by flow cytometric analysis [20]. RAW 264.7 macrophages were stimulated with LPS (1 μg/mL) and treated with CSE (0.02–0.06 mg dry biomass equivalents/mL) for 24 h; the LPS-treated control received no CSE. The cells were then stained with 500 nM CellROX™ Orange Reagent under dark conditions, followed by SYTOX™ Red Dead

Cell Stain to exclude non-viable cells. Fluorescence was analyzed using a CytoFLEX flow cytometer (Beckman Coulter, Brea, CA, USA). Intracellular ROS levels were quantified based on the mean fluorescence intensity (MFI) measured in the B585-A channel in viable cells. For graphical presentation, MFI values were normalized to the LPS-treated control and expressed as a percentage of the LPS-treated control.

2.7. Gene and protein expression analysis

Inflammation-related gene and protein expression levels were analyzed in RAW 264.7 macrophages stimulated with lipopolysaccharide (LPS, 1 μg/mL) and treated with CSE (0.02–0.06 mg dry biomass equivalents/mL) for 24 h; the LPS-treated control received no CSE [21]. Cells were seeded in 24-well plates at a density of 1×10^5 cells/well and incubated for 24 h prior to treatment. Total RNA was isolated using the AccuPrep® Universal RNA Extraction Kit (Bioneer, Daejeon, Korea), and RNA concentration was determined using a NanoDrop™ 2000 spectrophotometer (Thermo Fisher Scientific, Waltham, MA, USA). Complementary DNA (cDNA) was synthesized using AmpiRivert cDNA Synthesis Platinum Master Mix (GenDEPOT, Barker, TX, USA) according to the manufacturer's instructions. Semi-quantitative reverse transcription–polymerase chain reaction (RT-PCR) was performed using gene-specific primers listed in Supplementary Table S1. PCR amplification was carried out under the following conditions: initial denaturation at 95 °C for 5 min, followed by 30 cycles of denaturation at 95 °C for 30 s, annealing at 60 °C for 30 s, and extension at 72 °C for 30 s, with a final extension at 72 °C for 5 min. Amplified PCR products were separated on 1.5% agarose gels containing GelRed® nucleic acid stain (Komabiotech, Seoul, Korea), and band intensities were quantified using a Davinch-Gel™ imaging system (Young In Labplus, Yongin, Korea) with CLIQS software (TotalLab, Newcastle upon Tyne, UK). Relative band intensities were normalized to glyceraldehyde-3-phosphate dehydrogenase (*GAPDH*) and expressed relative to the LPS-treated control.

For protein expression analysis, cellular proteins were extracted using radioimmunoprecipitation assay (RIPA) buffer and quantified using a Bradford assay. Equal amounts of protein (10 μg) were separated on 10% SDS–polyacrylamide gels and transferred onto polyvinylidene fluoride (PVDF) membranes. Membranes were blocked with 5% (w/v) skim milk for 1 h at room temperature and incubated overnight at 4 °C with primary antibodies against NF-κB p65 (Santa Cruz Biotechnology, Dallas, TX, USA; Cat. No. sc-8008; 1:500), TNF-α (Santa Cruz Biotechnology; Cat. No. sc-52746; 1:500), iNOS (Santa Cruz Biotechnology; Cat. No. sc-7271; 1:500), IL-6 (Cell Signaling Technology, Danvers, MA, USA; Cat. No. 12912; 1:1000), IL-1β (Cell Signaling Technology; Cat. No. 12242; 1:1000), and β-actin (Santa Cruz Biotechnology; Cat. No. sc-47778; 1:1000). The

membranes were subsequently incubated with horseradish peroxidase (HRP)-conjugated secondary antibodies appropriate for the host species of the primary antibodies, including a mouse immunoglobulin G (IgG) κ light chain-binding protein secondary antibody (Santa Cruz Biotechnology; Cat. No. sc-516102; 1:1000) and a mouse anti-rabbit IgG-HRP secondary antibody (Santa Cruz Biotechnology; Cat. No. sc-2357; 1:1000), for 1 h at room temperature. Protein bands were visualized using enhanced chemiluminescence (ECL) and quantified using a KwikQuant Pro Multi-Image Analyzer (D1010, Kindle Bio, Greenwich, CT, USA). β-Actin was used as the loading control. Band intensities were measured from non-saturated bands, and no post-acquisition adjustment of brightness or contrast was applied to the blot images used for densitometric analysis.

2.8. Immunofluorescence staining analysis

Immunofluorescence staining was performed to evaluate LPS-induced NF-κB p65 nuclear accumulation in RAW 264.7 macrophages. Cells were seeded in 24-well plates at a density of 2×10^5 cells/well and stimulated with LPS (1 μg/mL) in the presence or absence of CSE (0.02–0.06 mg dry biomass equivalents/mL) for 24 h; the LPS-treated control received no CSE. After treatment, cells were washed three times with 1× phosphate-buffered saline (PBS, 300 μL/well, 5 min each) and fixed with 4% paraformaldehyde (200 μL/well) for 30 min at room temperature. The fixed cells were washed with 1× PBS and permeabilized with 0.1% Triton X-100 (200 μL/well) for 15 min. After washing, cells were blocked with 0.2% bovine serum albumin (BSA; 200 μL/well) for 1 h at room temperature.

The cells were then incubated overnight for 12 h with an anti-NF-κB p65 primary antibody diluted 1:800. After washing with 1× PBS, cells were incubated with Alexa Fluor™ 488 goat anti-mouse IgG (H+L) secondary antibody (Invitrogen, Thermo Fisher Scientific, Waltham, MA, USA; Cat. No. A11001) for 1 h under dark conditions. The cells were subsequently washed with 1× PBS and counterstained with 4′,6-diamidino-2-phenylindole (DAPI) diluted 1:1000 for 10 min under dark conditions. After a final wash with 1× PBS, fluorescence images were obtained using a fluorescence microscope. Fluorescence images were quantified using ImageJ software (National Institutes of Health, Bethesda, MD, USA), and NF-κB p65 nuclear accumulation was evaluated by measuring NF-κB p65 fluorescence intensity in DAPI-defined nuclear regions.

2.9. Statistical analysis

All cellular experiments were performed using three independent plates as biological replicates (n = 3), and cell-free biochemical assays were performed in three independent experiments unless otherwise stated.

When technical replicates were included within each plate, their values were averaged before statistical analysis, and each independent plate was treated as one biological replicate. Data are presented as the mean ± standard deviation (SD). Statistical analyses were performed using GraphPad Prism software (version 10.5.0; GraphPad Software Inc., San Diego, CA, USA). Comparisons between two groups were performed using an unpaired two-tailed Student's *t*-test. For comparisons among multiple groups, one-way analysis of variance (ANOVA) followed by Dunnett′s multiple comparisons test was used when each treatment group was compared with a single control group, whereas Tukey's multiple comparisons test was used for pairwise comparisons among multiple groups. For Supplementary Fig. S1, panels A and B were analyzed using unpaired two-tailed Student's t-tests, whereas panels C and D were analyzed using one-way ANOVA followed by Tukey's multiple comparisons test. $P < 0.05$ was considered statistically significant.

3. Results

3.1. Analysis of secondary metabolite content

TPC, TFC, and radical-scavenging activities of CSE are presented in Supplementary Fig. S1. The TPC of CSE was 9.0 mg GAE/g DM, which was 7.2% lower than that of the reference compound tannic acid (TA, 9.7 mg GAE/g DM); however, the difference was not statistically significant. The TFC of CSE was 8.3 mg QE/g DM, representing a 12.6% lower value than that of TA (9.5 mg QE/g DM; $P < 0.05$).

In the DPPH assay, radical-scavenging activity was highest in ascorbic acid (AA, 95.0%), followed by TA (55.0%) and CSE (30.0%). AA showed significantly higher activity than both TA and CSE ($P < 0.001$), and TA also showed significantly higher activity than CSE ($P < 0.01$). In the ABTS assay, AA exhibited the highest radical-scavenging activity (98.0%), followed by TA (60.0%) and CSE (55.0%). AA showed significantly higher activity than both TA and CSE ($P < 0.001$), whereas the difference between TA and CSE was not statistically significant.

3.2. Analysis of cell viability

The effects of CSE on the viability of RAW 264.7 macrophages are presented in Fig. 1. Treatment with CSE at concentrations ranging from 0 to 0.5 mg dry biomass equivalents/mL resulted in a concentration-dependent decrease in cell viability. Compared with the untreated control (NT), cell viability was maintained at approximately 95–98% in the 0.02–0.03 mg dry biomass equivalents/mL groups and remained above 92% at

0.06 mg dry biomass equivalents/mL, with no significant reduction observed at these concentrations. At 0.12 and 0.25 mg dry biomass equivalents/mL, cell viability decreased to approximately 82–85%. A statistically significant reduction compared with the NT group was observed at 0.25 mg dry biomass equivalents/mL ($P < 0.05$), while treatment with 0.5 mg dry biomass equivalents/mL further reduced cell viability to approximately 75% ($P < 0.001$; Fig. 1). Based on these results, CSE concentrations of 0.02–0.06 mg dry biomass equivalents/mL were selected for subsequent cellular assays to minimize the influence of cytotoxicity.

3.3. Analysis of nitrite accumulation

Nitrite accumulation, used as an indicator of nitric oxide (NO) production, in LPS-stimulated RAW 264.7 macrophages is presented in Fig. 2. LPS treatment increased nitrite accumulation by approximately 2.07-fold compared with the NT group. Co-treatment with CSE reduced nitrite levels by 10.6–32.7% compared with the LPS-treated group, with significant reductions observed at 0.02 mg dry biomass equivalents/mL ($P < 0.01$) and 0.06 mg dry biomass equivalents/mL ($P < 0.001$). The greatest reduction, 32.7%, was observed at 0.06 mg dry biomass equivalents/mL CSE (Fig. 2).

3.4. Intracellular ROS measurement by flow cytometry

Intracellular ROS levels in LPS-stimulated RAW 264.7 macrophages were analyzed by flow cytometry and are presented in Fig. 3. ROS-associated fluorescence based on MFI measured in the B585-A channel increased by approximately 3.35-fold in the LPS-treated group compared with the NT group (Fig. 3B, $P < 0.001$). When normalized to the LPS-treated control, ROS levels were 29.8% in the NT group and 100.0% in the LPS-treated group. Treatment with CSE reduced ROS levels to 95.2%, 78.4%, and 74.6% of the LPS-treated control at concentrations of 0.02, 0.03, and 0.06 mg dry biomass equivalents/mL, respectively. These values corresponded to reductions of 4.8%, 21.6%, and 25.4%, respectively, compared with the LPS-treated control. Significant reductions were observed at 0.02 mg dry biomass equivalents/mL ($P < 0.01$) and 0.06 mg dry biomass equivalents/mL ($P < 0.001$; Fig. 3B). Although the magnitude of reduction was relatively modest, CSE consistently decreased LPS-induced ROS-associated fluorescence, with the greatest reduction observed at 0.06 mg dry biomass equivalents/mL.

3.5. Evaluation of inflammation-related gene and protein expression

Inflammation-related gene and protein expression levels in LPS-stimulated RAW 264.7 macrophages

are presented in Figs. 4 and 5. LPS treatment significantly increased the mRNA expression of all evaluated genes compared with the NT group ($P < 0.001$; Fig. 4B–F). Compared with the LPS-treated group, CSE treatment reduced *iNOS* mRNA expression by 23.7–46.1% at concentrations of 0.02–0.06 mg dry biomass equivalents/mL (Fig. 4B). The mean expression of *IL-6* was nearly unchanged at 0.02 mg dry biomass equivalents/mL, with a reduction of 0.2%, but decreased by 4.9% and 13.1% at 0.03 and 0.06 mg dry biomass equivalents/mL, respectively (Fig. 4C). CSE also reduced *IL-1β* mRNA expression by 7.3–65.1%, with the greatest reduction observed at 0.06 mg dry biomass equivalents/mL (Fig. 4D). In addition, *TNF-α* and *NF-κB* mRNA expression decreased by 14.8–33.9% and 9.8–30.4%, respectively (Fig. 4E, F). Overall, the mean expression levels of all evaluated genes were lowest at 0.06 mg dry biomass equivalents/mL CSE.

Protein expression analysis showed that CSE also reduced inflammatory cytokine and mediator expression at the protein level, with the magnitude of reduction differing depending on the marker and concentration. Compared with the LPS-treated group, CSE decreased the protein expression levels of iNOS, IL-6, IL-1β, TNF-α, and NF-κB p65, with the greatest reductions generally observed at 0.06 mg dry biomass equivalents/mL (Fig. 5B–F). After normalization to β-actin, the protein expression levels of iNOS, IL-6, IL-1β, TNF-α, and NF-κB p65 were reduced by 42.1%, 21.2%, 66.1%, 18.8%, and 62.8%, respectively, at 0.06 mg dry biomass equivalents/mL CSE.

3.6. Immunofluorescence staining analysis

The intracellular localization of NF-κB p65 in LPS-stimulated RAW 264.7 macrophages is presented in Fig. 6. Treatment with CSE (0.02–0.06 mg dry biomass equivalents/mL) reduced the nuclear fluorescence intensity of NF-κB p65 by 10.1–57.1% compared with the LPS-treated group. The reduction at 0.02 mg dry biomass equivalents/mL was not statistically significant, whereas the greatest reduction was observed at 0.06 mg dry biomass equivalents/mL CSE ($P < 0.001$; Fig. 6B).

4. Discussion

The present findings demonstrate that CSE attenuated LPS-induced inflammatory responses in RAW 264.7 macrophages, accompanied by changes in oxidative stress-associated responses, nitrite accumulation, inflammatory cytokine and mediator expression, and NF-κB p65 nuclear accumulation. Polyphenols and flavonoids are representative antioxidant-related constituents commonly used to evaluate the functional potential

of plant- and microalgae-derived extracts [22,23]. Although CSE exhibited lower DPPH and ABTS radical-scavenging activities than the reference antioxidants, it contained measurable levels of polyphenols and flavonoids and reduced ROS-associated fluorescence under LPS-stimulated conditions. Because the compositional analysis in this study was limited to TPC and TFC measurements, the specific bioactive constituents responsible for these effects could not be identified. Therefore, the anti-inflammatory activity of CSE may involve mechanisms beyond direct radical-scavenging, rather than being explained solely by its antioxidant capacity. Consistent with this interpretation, phenolic compounds derived from natural sources have been reported to regulate inflammatory responses through oxidative stress-related signaling pathways, including NF-κB-associated responses [24,25]. Furthermore, CSE did not significantly reduce cell viability at concentrations of 0.02–0.06 mg dry biomass equivalents/mL, indicating that the observed anti-inflammatory effects were unlikely to result from nonspecific cytotoxicity [26].

ROS and NO are major mediators involved in the amplification of inflammatory signaling in LPS-stimulated macrophages [27–29]. In the present study, CSE reduced ROS-associated fluorescence intensity and nitrite accumulation, the latter of which was used as an indicator of NO production. These changes were accompanied by decreased *iNOS* mRNA and iNOS protein expression. Because iNOS is the primary enzyme responsible for inducible NO production during inflammatory responses, these findings suggest that the inhibitory effect of CSE on nitrite accumulation was associated with reduced iNOS expression. Although the reduction in ROS-associated fluorescence intensity was less pronounced than the changes observed in nitrite accumulation and inflammatory marker expression, CSE consistently reduced this signal across all tested concentrations. These findings suggest that the anti-inflammatory activity of CSE may be associated, at least in part, with attenuation of oxidative stress-associated responses under LPS-stimulated conditions.

NF-κB is a central transcription factor regulating the expression of pro-inflammatory cytokines and inflammatory mediators in activated macrophages [30]. In the present study, CSE treatment was associated with lower mean mRNA expression levels of *iNOS*, *IL-6*, *IL-1β*, *TNF-α*, and *NF-κB*, although the magnitude of the response varied among the evaluated targets and concentrations. In particular, *IL-6* mRNA expression remained nearly unchanged at 0.02 mg dry biomass equivalents/mL but decreased at higher CSE concentrations. CSE also decreased the protein expression of iNOS, IL-6, IL-1β, TNF-α, and NF-κB p65, with more pronounced reductions observed for IL-1β and NF-κB p65 than for IL-6 and TNF-α at the highest CSE concentration. These findings indicate that CSE modulated multiple inflammation-related cytokines and mediators in LPS-stimulated

macrophages. However, because NF-κB activation is mainly regulated by post-translational events, including IκBα phosphorylation and degradation, p65 phosphorylation, and nuclear translocation, reduced NF-κB mRNA expression alone is not sufficient to demonstrate direct inhibition of NF-κB signaling. Therefore, the decrease in NF-κB mRNA should be interpreted as a supportive marker rather than the primary mechanistic evidence.

Immunofluorescence analysis further demonstrated that CSE reduced NF-κB p65 nuclear accumulation. Because nuclear accumulation of NF-κB p65 reflects a key event associated with NF-κB pathway activation [31], this finding supports an association between CSE treatment and attenuation of NF-κB-associated inflammatory signaling in LPS-stimulated RAW 264.7 macrophages. Collectively, CSE reduced ROS-associated fluorescence intensity and nitrite accumulation, modulated the expression of multiple inflammation-related cytokines and mediators, and decreased NF-κB p65 nuclear accumulation. Nevertheless, this study has several limitations. First, the experiments were limited to an *in vitro* macrophage model. Second, the bioactive constituents responsible for the observed anti-inflammatory effects were not individually identified by chromatographic or mass spectrometric analyses. Third, upstream NF-κB signaling events, including IκBα phosphorylation and degradation, IKK activation, and p65 phosphorylation, were not directly investigated. Therefore, further studies involving purified bioactive fractions, liquid chromatography–mass spectrometry and high-performance liquid chromatography-based compositional analyses, upstream signaling analyses, and *in vivo* inflammatory models are required to clarify the molecular mechanisms and therapeutic potential of CSE.

5. Conclusion

This study demonstrated that *Coelastrella* sp. extract (CSE) attenuated LPS-induced inflammatory responses in RAW 264.7 macrophages. CSE reduced ROS-associated fluorescence intensity and nitrite accumulation, the latter of which was used as an indicator of nitric oxide production, and lowered the mean expression levels of multiple inflammation-related genes and proteins, although the magnitude of the response varied among targets and concentrations. CSE also reduced NF-κB p65 nuclear accumulation.

Collectively, these findings indicate that the anti-inflammatory activity of CSE was associated with attenuation of oxidative stress-associated responses, nitrite accumulation, inflammation-related marker expression, and NF-κB p65 nuclear accumulation.

Data availability

The processed data supporting the findings of this study are included in this article and its supplementary information files. Additional raw data, including densitometric quantification data, uncropped gel and blot images, flow cytometry files, and image analysis sheets, are available from the corresponding author upon reasonable request.

References

1. Bellanti, F. et al. Redox imbalance in inflammation: the interplay of oxidative and reductive stress. *Antioxidants* **14,** 656 (2025).
2. Mao, H., Zhao, X. & Sun, S. C. NF-κB in inflammation and cancer. *Cell. Mol. Immunol.* **22,** 811–839 (2025).
3. Mao, Y. Apoptotic cell-derived metabolites in efferocytosis-mediated resolution of inflammation. *Cytokine Growth Factor Rev.* **62,** 42–53 (2021).
4. Peng, M. et al. Macrophages: subtypes, distribution, polarization, immunomodulatory functions, and therapeutics. *MedComm* **6,** e70304 (2025).
5. Zhang, T., Ma, C., Zhang, Z., Zhang, H. & Hu, H. NF-κB signaling in inflammation and cancer. *MedComm* **2,** 618–653 (2021).
6. Duan, T., Du, Y., Xing, C., Wang, H. Y. & Wang, R. F. Toll-like receptor signaling and its role in cell-mediated immunity. *Front. Immunol.* **13,** 812774 (2022).
7. Yin, L., Wei, X., Zhang, Y., Lu, C. & Wang, H. Citrulline inhibits LPS-induced pyroptosis of RAW264.7 macrophages through NF-κB signaling pathway. *Immun. Inflamm. Dis.* **11,** e832 (2023).
8. Shimba, A., Ejima, A. & Ikuta, K. Pleiotropic effects of glucocorticoids on the immune system in circadian rhythm and stress. *Front. Immunol.* **12,** 706951 (2021).
9. Liang, J., Zhou, X. & Jiang, L. Targeting inflammatory cytokines in autoimmune diseases: mechanisms and therapeutic advances with antibody-based therapies. *Health Metab.* **2,** 8 (2025).
10. Eladl, S. N., Elnabawy, A. M. & Eltanahy, E. G. Recent biotechnological applications of value-added bioactive compounds from microalgae and seaweeds. *Bot. Stud.* **65,** 28 (2024).
11. Liu, Y., Liu, X., Cui, Y. & Yuan, W. Ultrasound for microalgal cell disruption and product extraction: a review. *Ultrason. Sonochem.* **87,** 106054 (2022).
12. Yusoff, I. M., Mat Taher, Z., Rahmat, Z. & Chua, L. S. A review of ultrasound-assisted extraction for plant bioactive compounds: phenolics, flavonoids, thymols, saponins and proteins. *Food Res. Int.* **157,**

111268 (2022).

13. Shraim, A. M., Ahmed, T. A., Rahman, M. M. & Hijji, Y. M. Determination of total flavonoid content by aluminum chloride assay: a critical evaluation. *LWT* **150,** 111932 (2021).
14. Pérez, M., Dominguez-López, I. & Lamuela-Raventós, R. M. The chemistry behind the Folin–Ciocalteu method for the estimation of (poly)phenol content in food: total phenolic intake in a Mediterranean dietary pattern. *J. Agric. Food Chem.* **71,** 17543–17553 (2023).
15. Gang, Y. et al. Optimising the DPPH assay for cell-free marine microorganism supernatants. *Mar. Drugs* **19,** 256 (2021).
16. Munteanu, I. G. & Apetrei, C. Analytical methods used in determining antioxidant activity: a review. *Int. J. Mol. Sci.* **22,** 3380 (2021).
17. Coulombier, N., Jauffrais, T. & Lebouvier, N. Antioxidant compounds from microalgae: a review. *Mar. Drugs* **19,** 549 (2021).
18. Ghasemi, M., Turnbull, T., Sebastian, S. & Kempson, I. The MTT assay: utility, limitations, pitfalls, and interpretation in bulk and single-cell analysis. *Int. J. Mol. Sci.* **22,** 12827 (2021).
19. Wu, X. Guidelines for anti-inflammatory assays in RAW264.7 cells. *Food Saf. Health* **3,** 128–136 (2025).
20. Marcantonio, E. et al. Zinc-limited *Mycobacterium tuberculosis* stimulate distinct responses in macrophages compared with standard zinc-replete bacteria. *Infect. Immun.* **93,** e00578-24 (2025).
21. Park, S. et al. Pharmacological evaluation of araliadiol as a novel anti-inflammatory agent in LPS-induced RAW 264.7 cells. *Biomedicines* **13,** 1408 (2025).
22. Bertelli, A. et al. Polyphenols: from theory to practice. *Foods* **10,** 2595 (2021).
23. Kiss, A. et al. Comparative study on antioxidant capacity of diverse food matrices: applicability, suitability and inter-correlation of multiple assays to assess polyphenol and antioxidant status. *Antioxidants* **14,** 317 (2025).
24. Dini, I. & Grumetto, L. Recent advances in natural polyphenol research. *Molecules* **27,** 8777 (2022).
25. Chojnacka, K. & Lewandowska, U. The influence of polyphenol-rich extracts on the production of pro-inflammatory mediators in macrophages. *J. Physiol. Pharmacol.* **72,** 167–176 (2021).
26. Khalef, L., Lydia, R., Filicia, K. & Moussa, B. Cell viability and cytotoxicity assays: biochemical elements and cellular compartments. *Cell Biochem. Funct.* **42,** e4007 (2024).
27. Xu, R., Ma, L., Chen, T. & Wang, J. Sophorolipid suppresses LPS-induced inflammation in

RAW264.7 cells through the NF-κB signaling pathway. *Molecules* **27,** 5037 (2022).

28. Oun, A. et al. Characterization of lipopolysaccharide effects on LRRK2 signaling in RAW macrophages. *Int. J. Mol. Sci.* **24,** 1644 (2023).
29. Mfotie Njoya, E., Tabakam, G. T., Chukwuma, C. I., Mashele, S. S. & Makhafola, T. J. Phytoconstituents of *Androstachys johnsonii* Prain prevent reactive oxygen species production and regulate the expression of inflammatory mediators in LPS-stimulated RAW 264.7 macrophages. *Antioxidants* **13,** 401 (2024).
30. Mussbacher, M., Derler, M., Basílio, J. & Schmid, J. A. NF-κB in monocytes and macrophages – an inflammatory master regulator in multitalented immune cells. *Front. Immunol.* **14,** 1134661 (2023).
31. Zhao, Z. et al. Artemvulactone E isolated from *Artemisia vulgaris* L. ameliorates lipopolysaccharide-induced inflammation in both RAW264.7 and zebrafish model. *Front. Pharmacol.* **15,** 1415352 (2024).

Acknowledgements

This work was supported by Korea Environment Industry & Technology Institute (KEITI) through the 'Project to make multi-ministerial national biological research resources more advanced', funded by the Ministry of Climate, Energy and Environment (MCEE) (RS-2021-KE001788), and a grant (No. NNIBR20261107) from the Nakdonggang National Institute of Biological Resources (NNIBR).

Author contributions

Su Jeong Hwang: Conducted the experiments, acquired and analyzed the data, prepared the figures, and drafted the manuscript. Ju Hwan Lee: Contributed to the experimental design, laboratory analyses, and data interpretation. Jong Hyun Oh: Developed the experimental design, conducted laboratory analyses, acquired data, and contributed to the writing and revision of the manuscript. Do Hyeon Jin: Assisted in experimental investigation, data interpretation, and visualization of the results. Seung Won Nam: Contributed to the experimental design, laboratory analyses, and data interpretation. Jin Woo Kim: Conceived and supervised the study, contributed to the experimental design and interpretation of the data, and critically reviewed and finalized the manuscript. Sunhye Lee: Supervised the research, provided methodological guidance, coordinated the experimental work, and reviewed and revised the manuscript. All authors read and approved the final version of the manuscript.

Competing interests

The authors declare no competing interests.

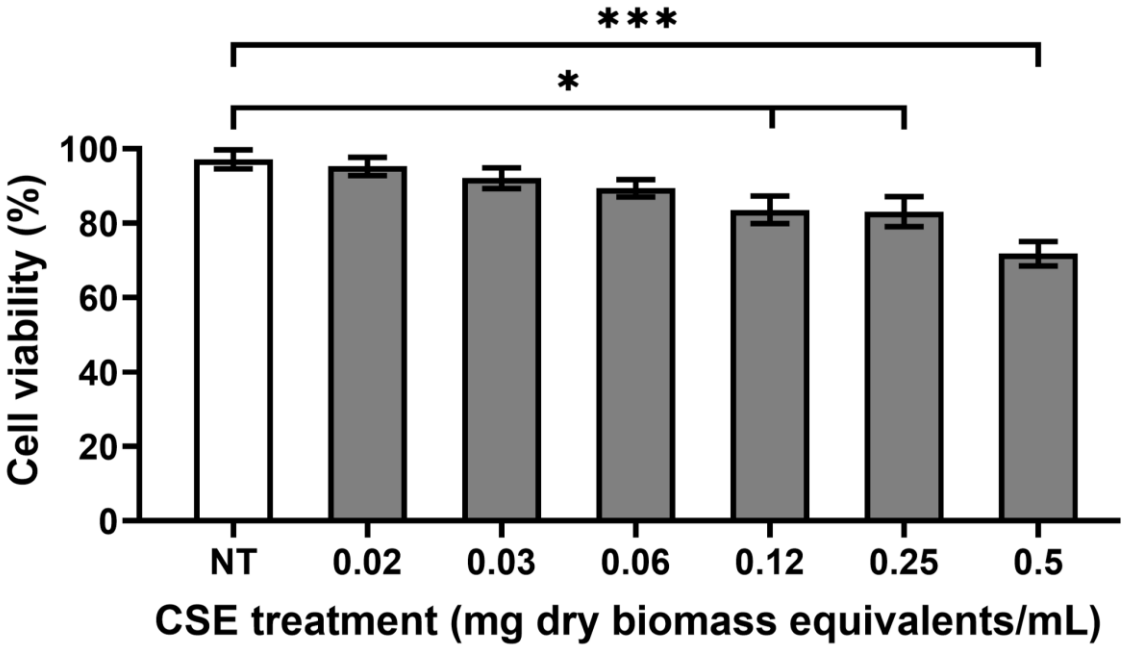


Fig. 1. Effects of *Coelastrella* sp. extract (CSE) on the viability of RAW 264.7 macrophages. Cells were treated with CSE (0–0.5 mg dry biomass equivalents/mL) for 24 h, and cell viability was determined using the MTT assay. Cell viability was expressed as a percentage of the untreated control (NT). Data are presented as the mean ± SD of three independent plates used as biological replicates ($n = 3$). Statistical analysis was performed using one-way ANOVA followed by Dunnett′s multiple comparisons test. *$P < 0.05$ and ***$P < 0.001$ compared with the NT group.

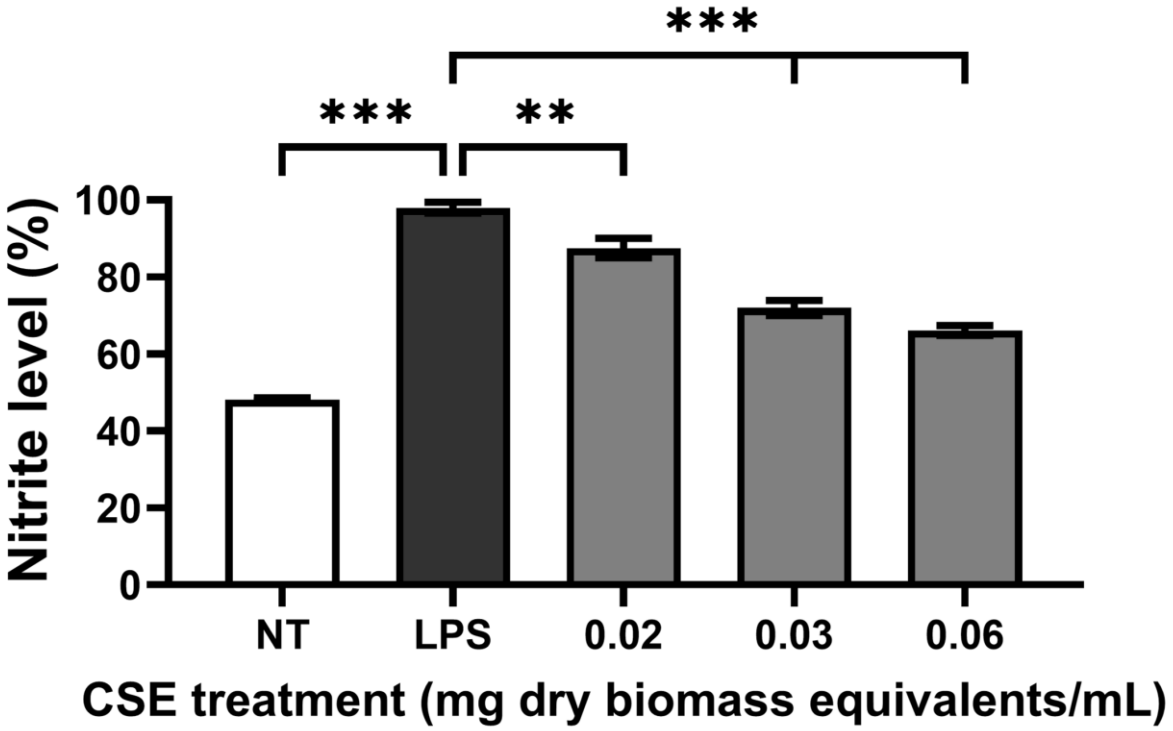


Fig. 2. Effects of *Coelastrella* sp. extract (CSE) on nitrite accumulation as an indicator of nitric oxide (NO) production in LPS-stimulated RAW 264.7 macrophages. Cells were stimulated with LPS (1 μg/mL) and treated with CSE (0.02–0.06 mg dry biomass equivalents/mL) for 24 h. Nitrite accumulation was measured using the Griess assay and expressed as a percentage of the LPS-treated control. Data are presented as the mean ± SD of three independent plates used as biological replicates ($n = 3$). Statistical analysis was performed using one-way ANOVA followed by Dunnett′s multiple comparisons test. $^{**}P < 0.01$ and $^{***}P < 0.001$ compared with the LPS-treated control.

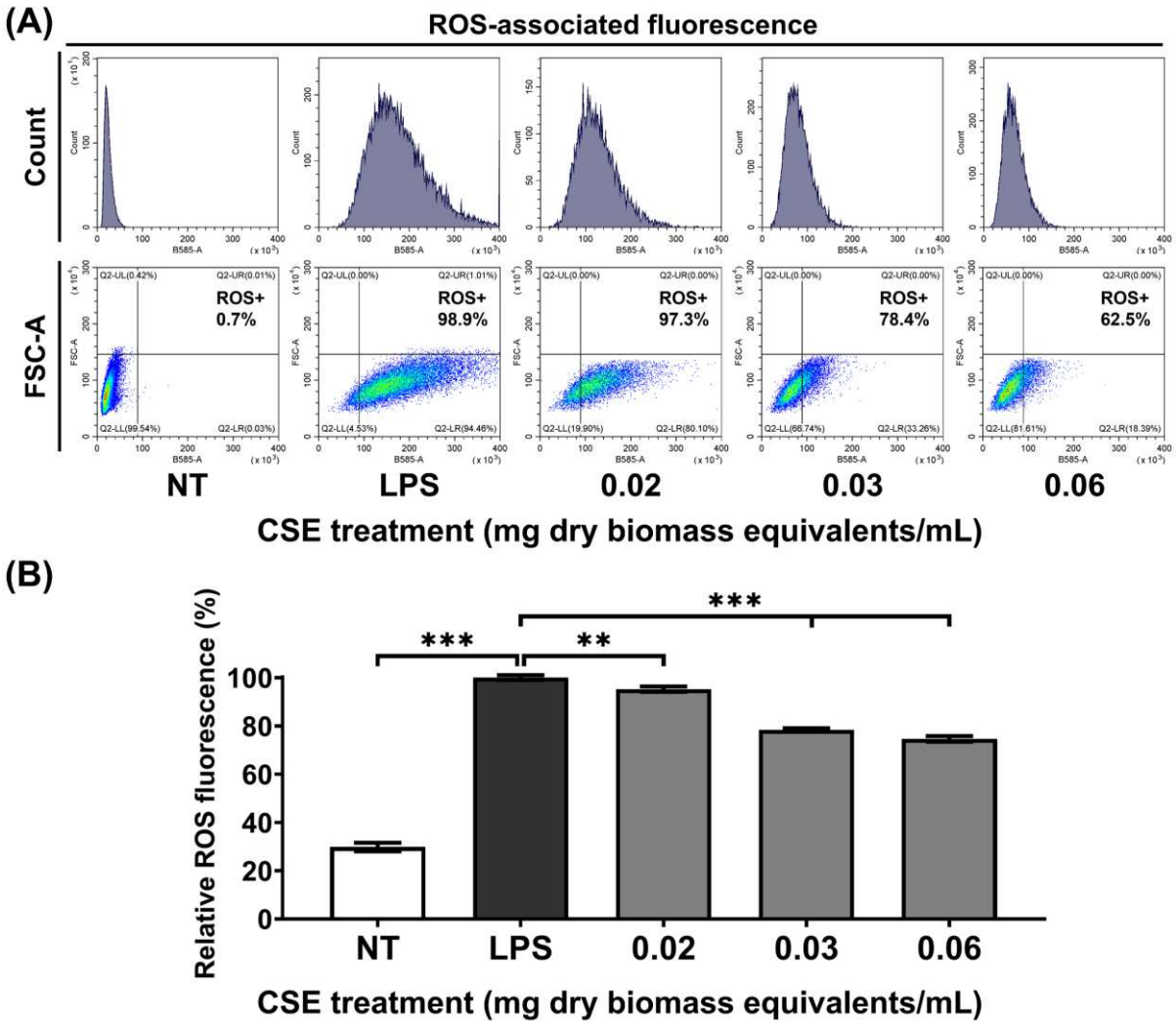


Fig. 3. Effects of *Coelastrella* sp. extract (CSE) on intracellular reactive oxygen species (ROS)-associated fluorescence in LPS-stimulated RAW 264.7 macrophages. Cells were stimulated with LPS (1 μg/mL) and treated with CSE (0.02–0.06 mg dry biomass equivalents/mL) for 24 h. (A) Representative flow cytometry histograms and dot plots showing ROS-associated fluorescence measured in the B585-A channel in viable cells. The fluorescence channel and gating strategy are indicated in the representative plots, and gate percentages indicate the proportion of ROS-positive cells in each representative dot plot. (B) Quantitative analysis of intracellular ROS levels based on mean fluorescence intensity (MFI) measured in the B585-A channel, expressed as a percentage of the LPS-treated control. Data are presented as the mean ± SD of three independent plates used as biological replicates ($n = 3$). Statistical analysis was performed using one-way ANOVA followed by Dunnett′s multiple comparisons test. $^{**}P < 0.01$ and $^{***}P < 0.001$ compared with the LPS-treated control.

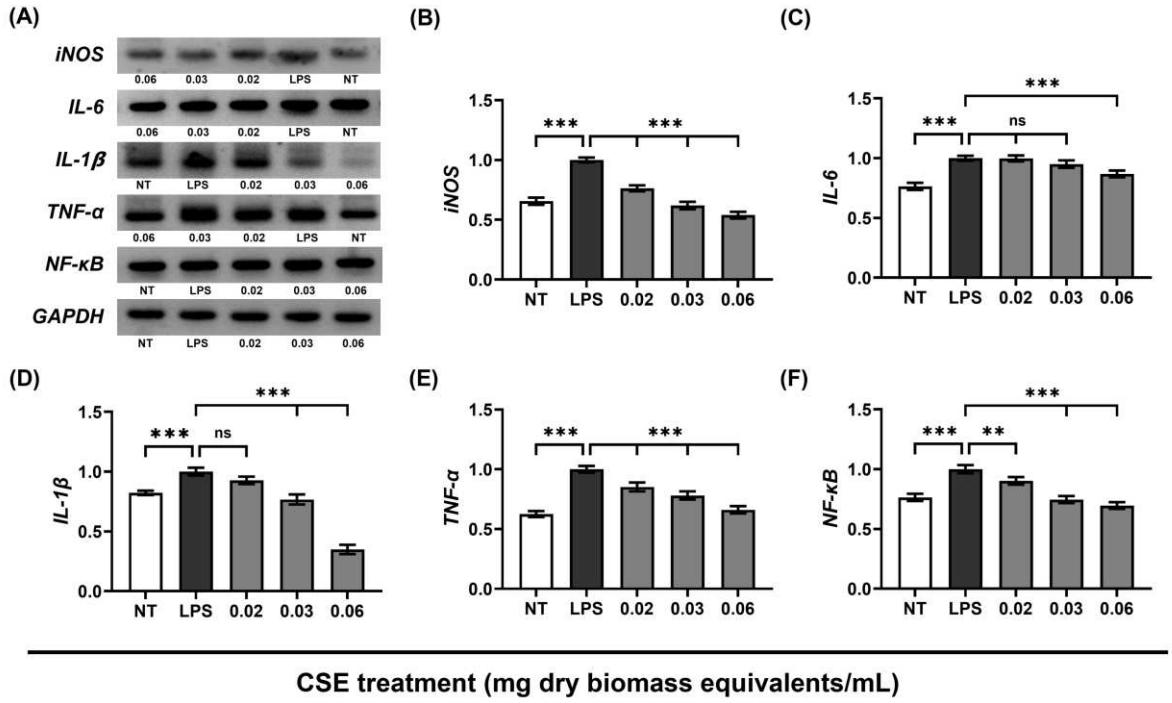


Fig. 4. Effects of *Coelastrella* sp. extract (CSE) on the expression of inflammation-related genes in LPS-stimulated RAW 264.7 macrophages. Cells were stimulated with LPS (1 μg/mL) and treated with CSE (0.02–0.06 mg dry biomass equivalents/mL) for 24 h. (A) Representative semi-quantitative RT-PCR bands. The representative band rows were cropped from separate full-length gels and assembled with white space between rows. Full-length gel images are provided in Supplementary Fig. S2. Relative mRNA expression levels of *iNOS* (B), *IL-6* (C), *IL-1β* (D), *TNF-α* (E), and *NF-κB* (F). Gene expression levels were normalized to *GAPDH* and expressed relative to the LPS-treated control. Data are presented as the mean ± SD of three independent plates used as biological replicates ($n = 3$). Statistical analysis was performed using one-way ANOVA followed by Dunnett's multiple comparisons test. ns, not significant; *$P < 0.05$, **$P < 0.01$, and ***$P < 0.001$ compared with the LPS-treated control. The representative gel images are presented in their native orientation, with the actual sample order indicated for each band row. Individual lanes were not rearranged.

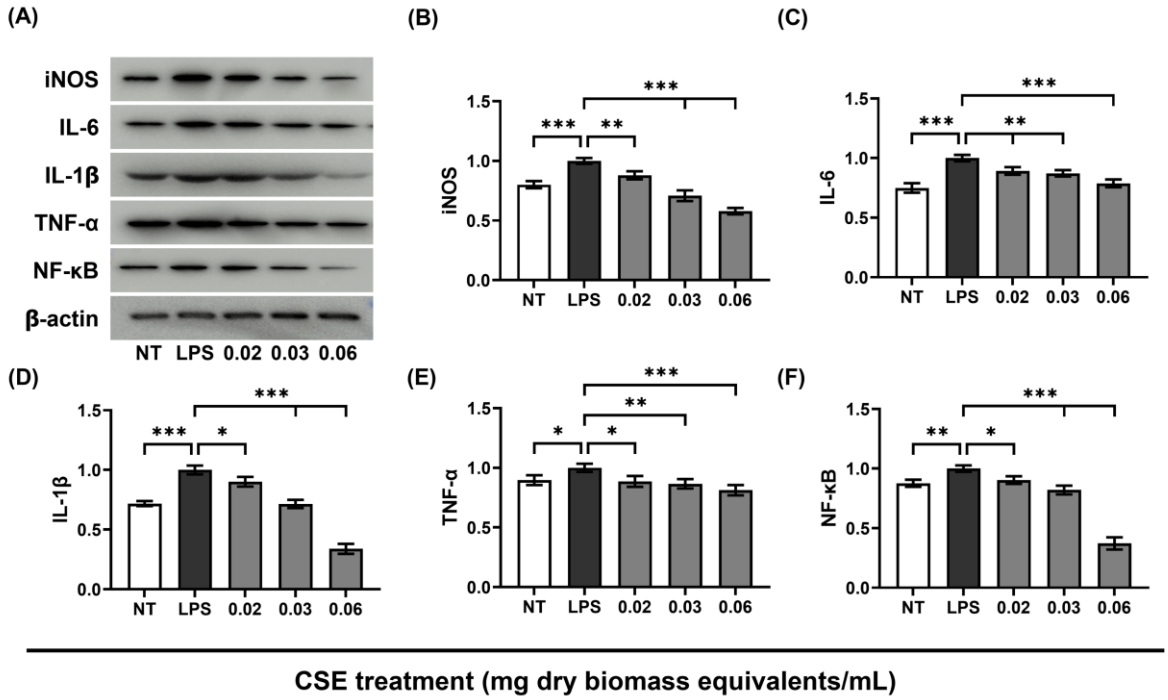


Fig. 5. Effects of *Coelastrella* sp. extract (CSE) on the expression of inflammation-related proteins in LPS-stimulated RAW 264.7 macrophages. Cells were stimulated with LPS (1 μg/mL) and treated with CSE (0.02–0.06 mg dry biomass equivalents/mL) for 24 h. **(A)** Representative Western blot bands. The blots for iNOS, IL-6, IL-1β, TNF-α, NF-κB p65, and β-actin were obtained from separate membranes using the same set of protein samples loaded in the same group order. Representative band rows were cropped from the respective full-length blots and grouped for presentation with white space between rows. Original full-length blot images for each membrane are presented in Supplementary Fig. S3. Relative protein expression levels of iNOS (B), IL-6 (C), IL-1β (D), TNF-α (E), and NF-κB p65 (F). Protein expression levels were normalized to β-actin and expressed relative to the LPS-treated control. Data are presented as the mean ± SD of three independent plates used as biological replicates ($n = 3$). Statistical analysis was performed using one-way ANOVA followed by Dunnett's multiple comparisons test. ns, not significant; *$P < 0.05$, **$P < 0.01$, and ***$P < 0.001$ compared with the LPS-treated control.

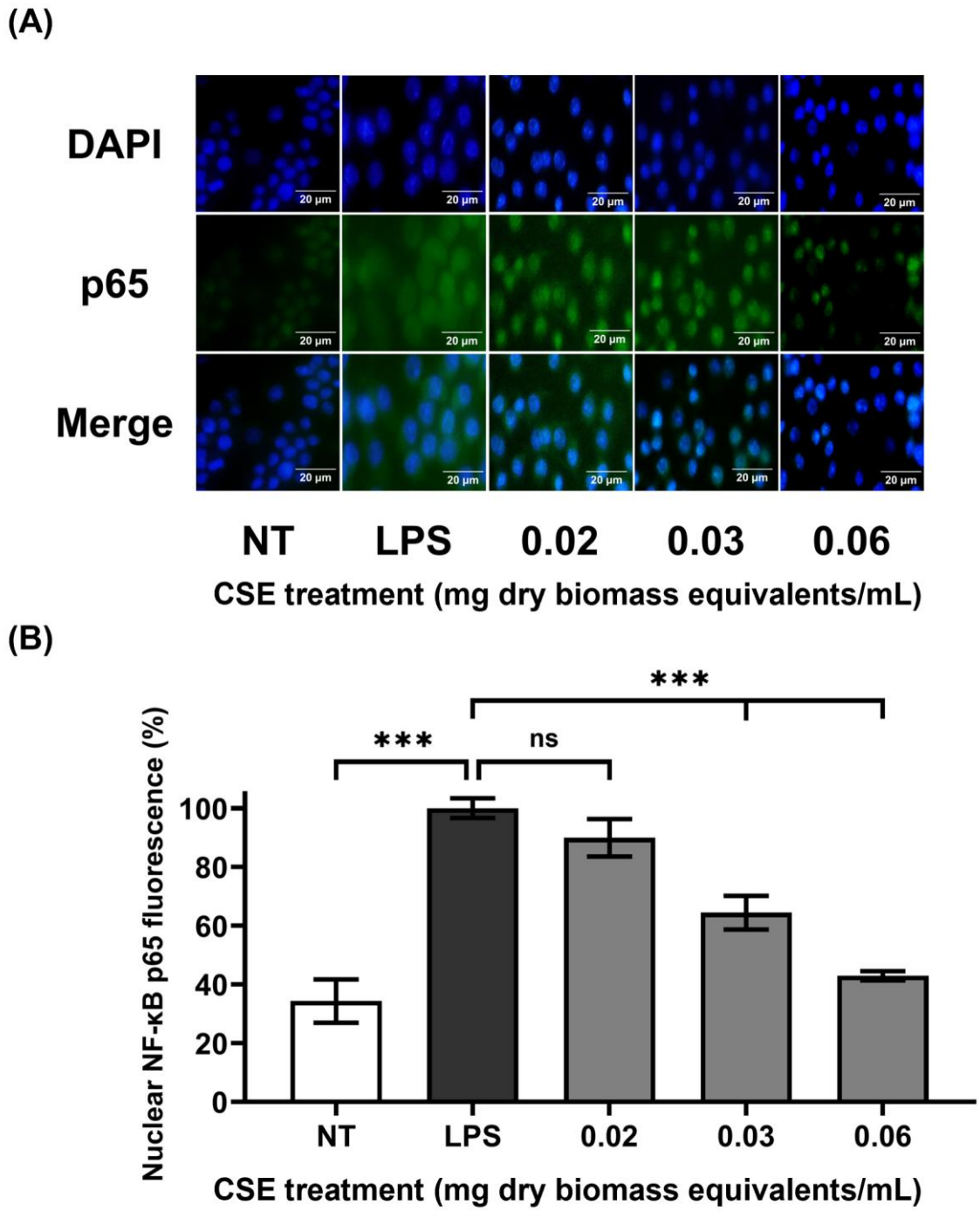


Fig. 6. Effects of *Coelastrella* sp. extract (CSE) on NF-κB p65 nuclear accumulation in LPS-stimulated RAW 264.7 macrophages. Cells were stimulated with LPS (1 μg/mL) and treated with CSE (0.02–0.06 mg dry biomass equivalents/mL) for 24 h. (A) Representative immunofluorescence images showing DAPI-stained nuclei (blue), NF-κB p65 immunofluorescence (green), and merged images. Scale bar = 20 μm. (B) Quantitative analysis of nuclear NF-κB p65 fluorescence intensity in DAPI-defined nuclear regions, expressed as a percentage of the LPS-treated control. Data are presented as the mean ± SD of three independent plates used as

biological replicates (n = 3). Statistical analysis was performed using one-way ANOVA followed by Dunnett′s multiple comparisons test. ns, not significant; ***P < 0.001 compared with the LPS-treated control.

Supplementary Files

This is a list of supplementary files associated with this preprint. Click to download.

- SupplementaryMaterial.pdf